

11

Multi-tube arrays

11.1 Limited streamer tubes

Despite their successful use in many experimental setups, gaseous detectors with multi-wire geometry potentially suffer from a reliability problem, since the accidental rupture of a single wire may cause the malfunctioning of a large part if not all of the system. Modular designs, as used for jet chambers, may limit the extent of the damage; nevertheless, the failure of one sector affects the whole experiment. Various technologies have been devised to repair a damaged detector; in general they require the dismounting of the setup, which is particularly difficult if the device is embedded in other components. This led to the development of detectors with each anode enclosed in a box or cylindrical tube protecting the surrounding elements from a local failure; one of them, the drift tube, is described in Chapter 9.

Originally developed as a way to limit the photon- and electron-mediated propagation of avalanches between adjacent wires in electromagnetic calorimeters, the cube lattice MWPC had each anode wire enclosed in an array of cathodes of rectangular cross section (Battistoni *et al.*, 1979b); the coordinates along the wire are measured by recording the induced charge profile on strips perpendicular to the anodes (Battistoni *et al.*, 1978). The early design made use of U-shaped aluminium profiles for the cathodes, with the open side covered by a resistive electrode to permit detection of the induced signals. Further development led to the use of extruded plastic profiles with controlled resistivity, with readouts of both coordinates on external sensing strips.

In systematic studies of performances with single-wire tubes, very large signals were observed using thick anode wires and large fractions of hydrocarbons as gas fillings; their origin was attributed to a transition from proportional avalanche to a streamer, limited in extension towards the cathode by the decreasing field in a process analogous to the self-quenching streamer mechanism described in Section 7.8 (Battistoni *et al.*, 1979a). A comparison of counting characteristics

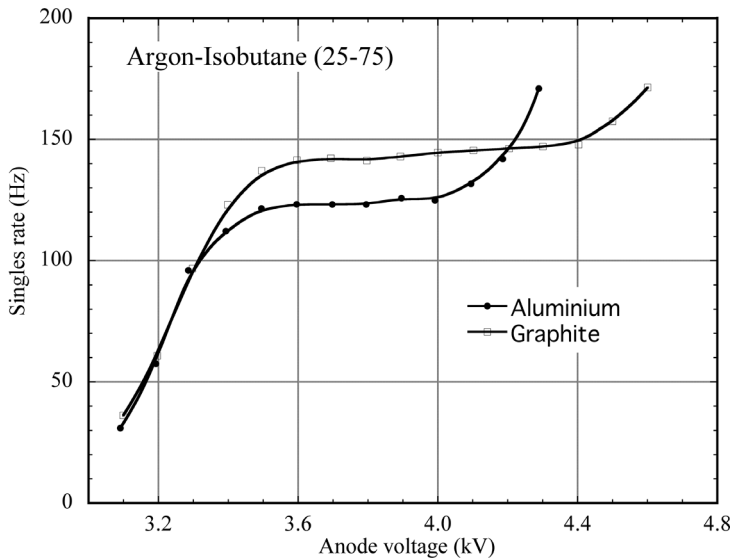


Figure 11.1 Comparison of singles counting rates for streamer tubes with graphite and aluminium cathodes (Battistoni *et al.*, 1983). By kind permission of Elsevier.

measured with metallic and resistive cathodes provides longer efficiency plateaux with the second option, probably due to the suppression of photon-mediated electron extraction from the cathodes, Figure 11.1 (Battistoni *et al.*, 1983).

Named plastic streamer tubes (PST) and built using large plates of extruded plastic profiles with resistive coatings, the detectors have been massively used in low- and medium-rate experiments requiring very large detection areas, as the NUSEX proton decay experiment under Mont Blanc (Battistoni *et al.*, 1986), MACRO at Gran Sasso (Ambrosio *et al.*, 2002), UA1 (Bauers *et al.*, 1987) and DELPHI experiments at CERN (Golovatyuk *et al.*, 1985).

Figure 11.2 shows schematically the construction of a PST module for the Mont Blanc experiment, with two-dimensional readout on external strips, and Figure 11.3 is a detailed view of the detector (Iarocci, 1983). A recording of charge profiles induced on external strips or pads is exploited to achieve localization; requiring rather inexpensive readout electronics, owing to the large signals obtained in the limited streamer operation, the tubes provide sub-mm localization accuracies in the direction of the anode wires. The amount and space distribution of the signals depend on detector geometry, cathode resistivity, distributed capacitance and amplifiers time constants; Figure 11.4 is a measurement of the fractional induced charge, or cathode transparency, as a function of the electrode surface resistivity (Battistoni *et al.*, 1982).

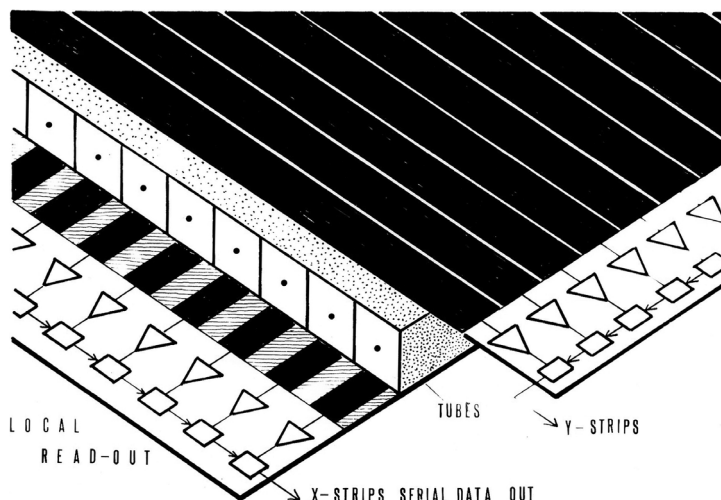


Figure 11.2 Schematics of a plastic streamer module (Iarocci, 1983). By kind permission of Elsevier.

While the transparency improves with the increase in resistivity, the rate capability of the detector can be affected by the accumulation of surface charges, modifying the field. Figure 11.5 is an example of charge measured as a function of rate, given in counts per cm of anode wire, for a detector with a cathode resistivity of about $50 \text{ k}\Omega/\text{square}$ (Fujii *et al.*, 1984); the gain drops above a particle flux of a few KHz per cm.

Many authors have analysed the process of charge induction through resistive electrodes (Battistoni *et al.*, 1978; Golovatyuk *et al.*, 1985; Fujimoto *et al.*, 1986); the subject is covered in more details in Chapter 12, which describes the development of resistive plate chambers.

11.2 Drift tubes

Named drift tubes, or straws in their lighter version, arrays of individual cylindrical proportional counters with metallic or low-resistivity cathodes solve the problem of both reliability encountered with multi-wire systems, and the rate limitations of resistive streamer tubes. Assembled in several staggered layers, as shown schematically in Figure 11.6, and with the measurement of drift time on each tube, they provide ambiguity-free reconstruction of tracks with good accuracy.

An early prototype, consisting of two planes of staggered proportional counter tubes operated in the proportional amplification mode, was built in the early eighties using 0.5 mm thick aluminium tubes, 1 m long and 3 mm in diameter, and tested up to a flux above 10^6 particles/s and mm of wire (Hammarström *et al.*,

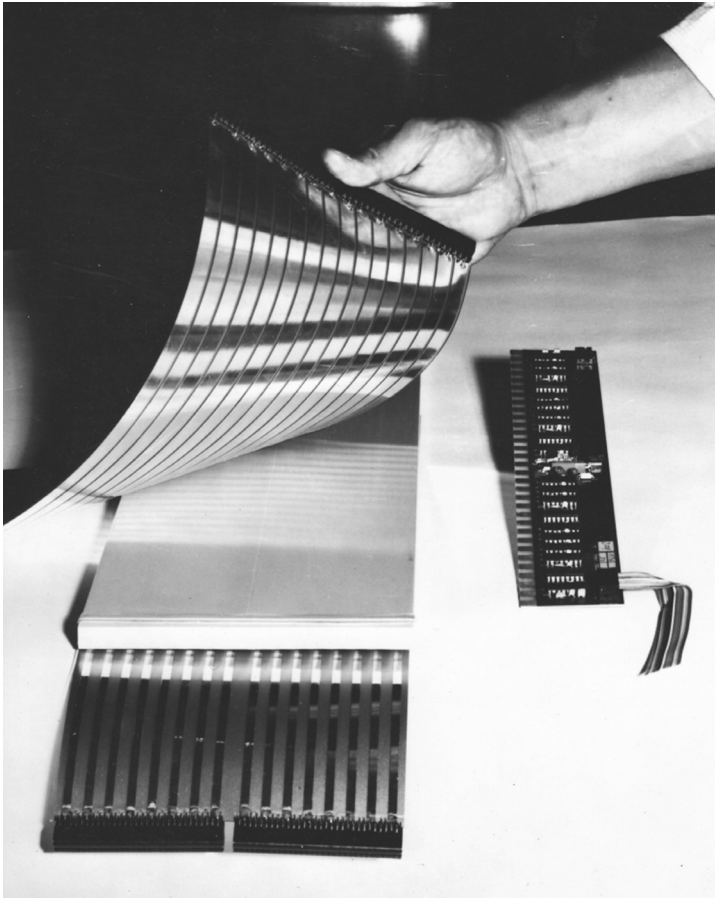


Figure 11.3 Detailed view of one end of the PST (Iarocci, 1983). By kind permission of Elsevier.

1980b). The technology evolved over the years, with the construction of detectors deploying thousand of tubes, usually assembled in self-supporting modules. For applications as muon detectors, where multiple scattering is not a major concern, both the tube walls and the supporting structure can be rather sturdy; this permits one to operate the tubes at pressures higher than atmospheric, improving the localization accuracy.

To exploit the intrinsic good localization properties of drift tubes, particularly for large systems, thorough position, gain and space–time correlation monitoring are essential, suggesting the name monitored drift tubes (MDT) for the detector (Biscossa *et al.*, 1999). Built in large quantity for CERN’s ATLAS barrel and end-cap muon spectrometers, the tubes have cathodes made of 400 μm thick aluminium tubes, 3 cm in diameter, and 50 μm anode wires held in place by

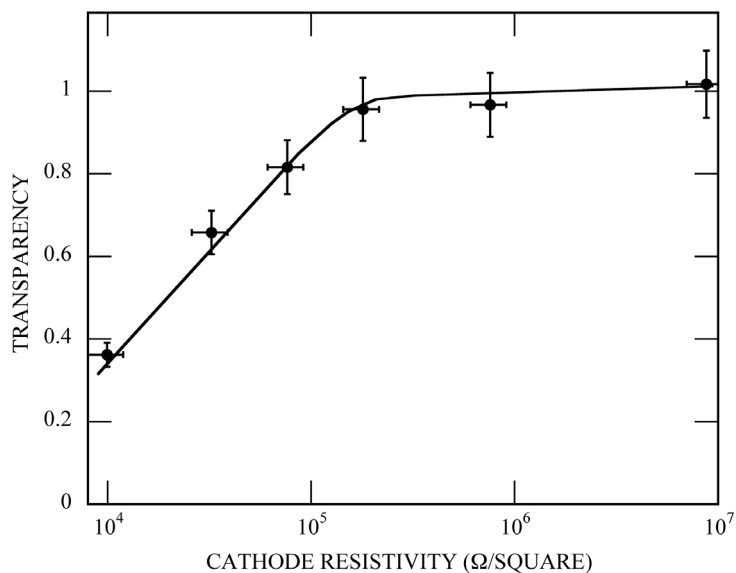


Figure 11.4 Cathode electrical transparency as a function of surface resistivity for 1 cm wide pickup strips (Battistoni *et al.*, 1982). By kind permission of Elsevier.

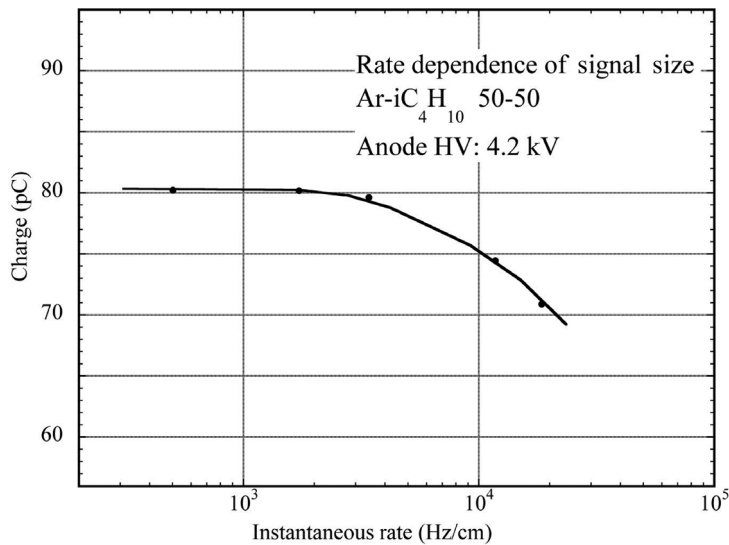


Figure 11.5 PST signal charge dependence from particles rate (Fujii *et al.*, 1984). By kind permission of Elsevier.

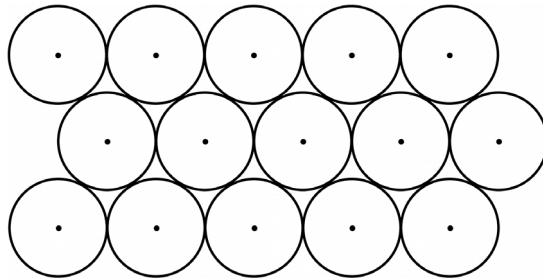


Figure 11.6 Schematic of a stack of staggered drift tubes.

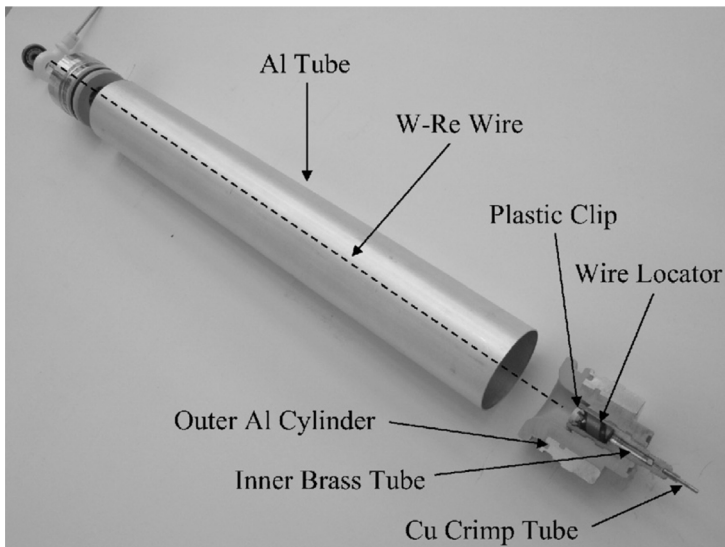


Figure 11.7 Exploded view of a MDT counter (Adorisio *et al.*, 2007). By kind permission of Elsevier.

insulating end-plugs providing the mechanical strength and gas inlets (Figure 11.7); Figure 11.8 is a detailed view of the wire-holding end-plug (Adorisio *et al.*, 2007). In the event of a failure, the anode wire can be replaced with a procedure described in the previous reference.

For installation in the experiment, the tubes are assembled in multi-layer modules; Figure 11.9 show schematically the structure of one ATLAS MDT barrel chamber (Riegler, 2002a). End-cap modules, similar in design, have a trapezoidal shape with tubes varying in length from 1.3 to 6.3 m (Bensinger *et al.*, 2002; Borisov *et al.*, 2002).

During construction, the absolute position of each anode wire is certified with 20 μm accuracy with respect to reference marks by a system of X-ray tomography

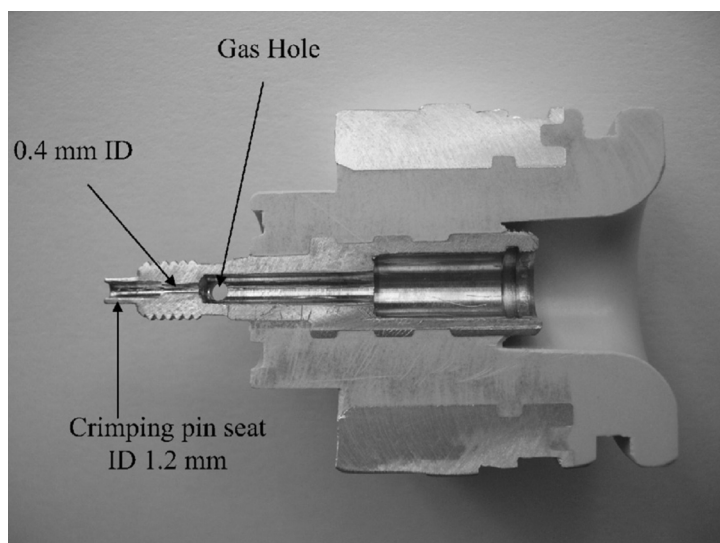


Figure 11.8 Detailed view of the MDT wire holder end-plug (Adorisio *et al.*, 2007). By kind permission of Elsevier.

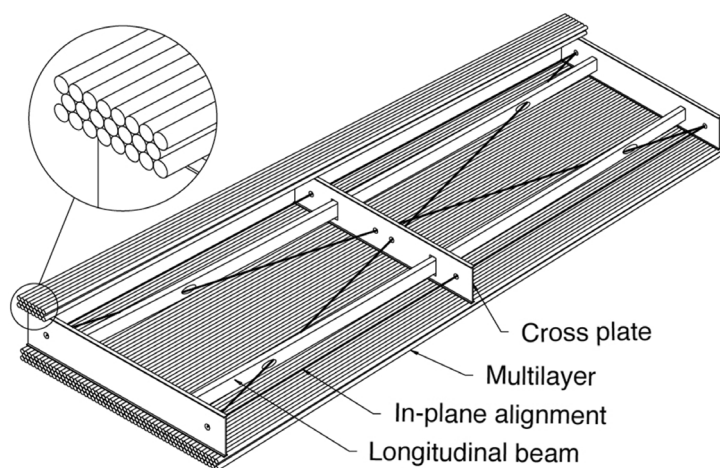


Figure 11.9 MDT module for the ATLAS barrel muon spectrometer (Riegler, 2002a). By kind permission of Elsevier.

(Schuh *et al.*, 2004); optical and capacitive alignment systems, complemented by calibrations on cosmic rays, permit one to reduce the system position errors to a few tens of μm (Cerutti, 2004; Dubbert *et al.*, 2007a). The picture in Figure 11.10 shows a module and monitoring system during assembly. About 1200 modules, for



Figure 11.10 Construction and alignment of a MDT module. Picture CERN (2004).

a total of 370 000 drift tubes, have been built by different collaborating institutes and are operational in the experiment.

While the best position accuracies could be obtained with a mixture of Ar/N₂/CH₄, owing to its saturated drift velocity over most of the drift length (Riegler *et al.*, 2000), due to ageing problems encountered the ATLAS MDTs are operated with argon-CO₂ (93–7) at 3 bars, resulting in a more pronounced non-linearity of the space–time correlation and a moderate loss in position accuracy (Aleksa *et al.*, 2002). However, the space–time correlation is affected by the counting rate, due to the accumulation of positive ions and the resulting space–charge field distortion, a process discussed in Section 7.7. The measured position accuracy of the MDT as a function of distance from the anode, both for low and high rates (about 1.4 kHz/cm of wire), are compared in Figure 11.11; the lines correspond to a fit with a model calculation (Aleksa *et al.*, 2002).

Mounted on the coils of the toroidal magnets of the spectrometer, the MDTs operate in a stray magnetic field up to 0.4 T; the position-dependent distortions introduced in the space–time correlation have been thoroughly modelled to achieve the required tracking accuracy (Dubbart *et al.*, 2007b).

An improved design of the MDT, with a tube diameter reduced from 30 to 15 mm, has been developed to cope with the higher counting rates expected after the upgrade of CERN's LHC (Bittner *et al.*, 2011).

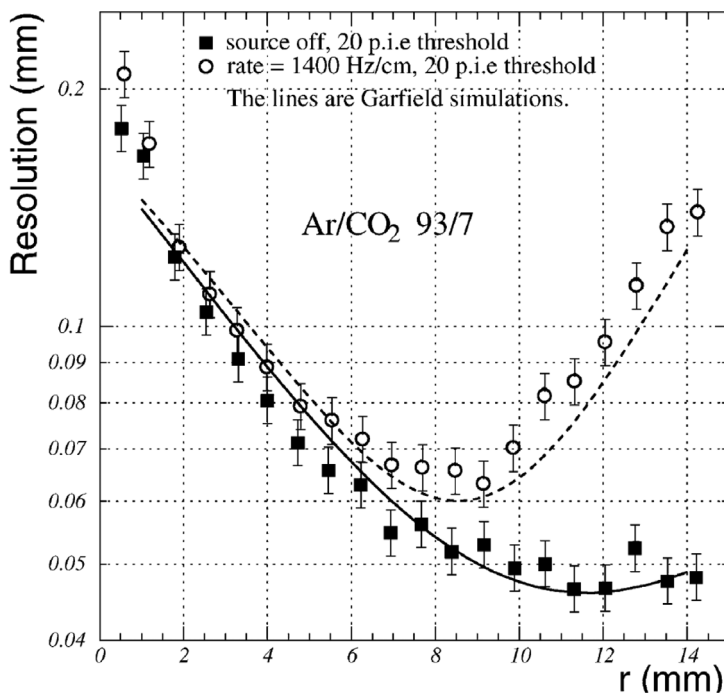


Figure 11.11 MDT space resolution as a function of distance from the wire for two source rates (Aleksa *et al.*, 2002). By kind permission of Elsevier.

11.3 Straw tubes

A limitation for the use of the drift tubes described in the previous section lies in the thickness of the cathodes; acceptable for high-energy muon detection, it causes a deterioration of tracking accuracy for lower momentum particles. The development of techniques capable of manufacturing single-wire counters with thin plastic walls, the so-called straws, permits the realization of large arrays of light detectors, particularly suited for the construction of cylindrical trackers in colliding beam setups (Baringer *et al.*, 1987). Figure 11.12 is a schematic cross section of one of the first large arrays of straw drift chambers for the MARK II detector, including 552 single-wire tubes; made with thin polymer cathodes, metal-coated on the inner side, the straws typically have a thickness of 50 to 100 μm , corresponding to a few tens of a per cent of radiation length (Ford *et al.*, 1987). Planar assemblies of straw arrays, usually glued together in modules to improve mechanical stability, have been used in many experiments (Arai *et al.*, 1996; Armstrong *et al.*, 1999; Ogren, 1995; Fourletov, 2004; Bychkov *et al.*, 2006; Bachmann *et al.*, 2004).

Several technologies have been developed to permit the industrial manufacturing of very large quantities of detectors. Figure 11.13 shows the method used for

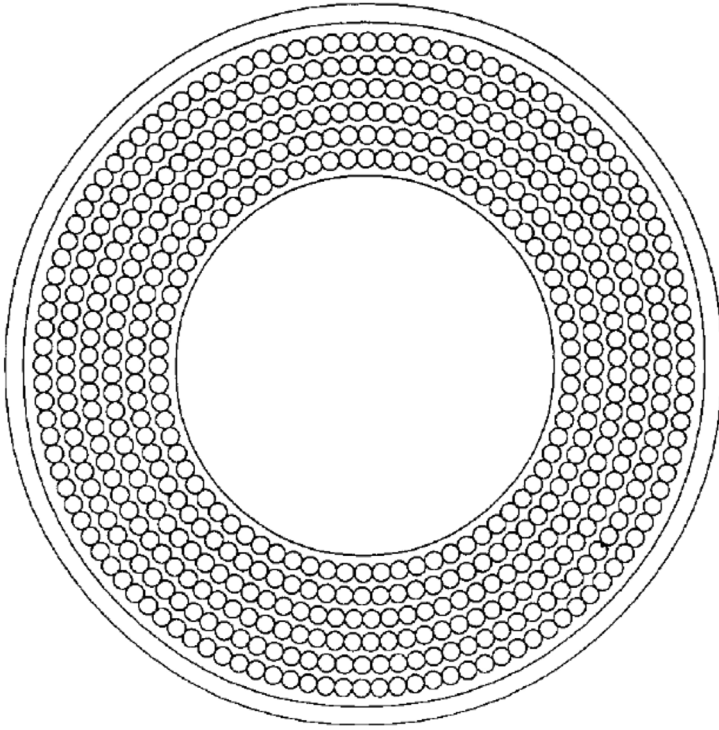


Figure 11.12 Schematic cross section of the MARK II cylindrical straw detector at PEP (Ford *et al.*, 1987). By kind permission of Elsevier.

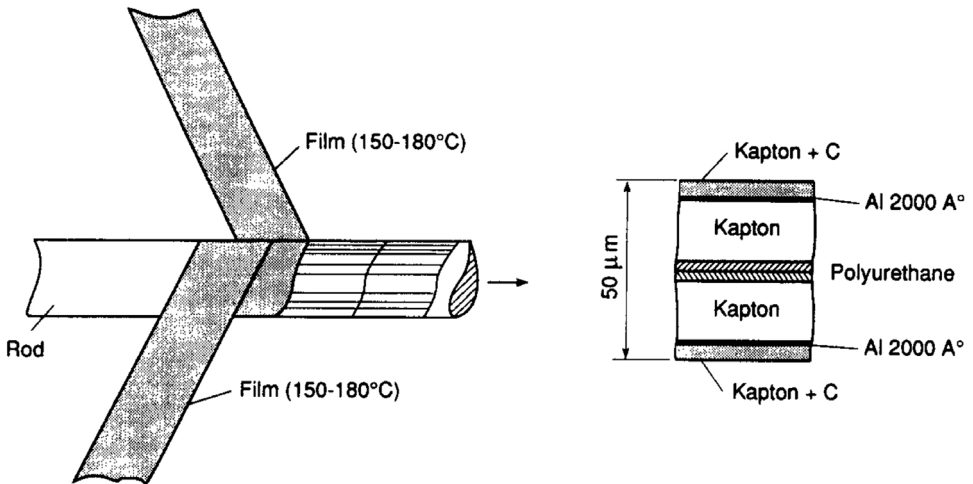


Figure 11.13 Straw manufacturing method, winding two polymer films around a core (Akesson *et al.*, 2004a). By kind permission of Elsevier.



Figure 11.14 Two-layer structure of the straws for COMPASS (Bychkov *et al.*, 2006). By kind permission of Elsevier.

the straws of the ATLAS Transition Radiation Tracker (Akesson *et al.*, 2004a): two thin polymer films are wound in spirals on a precisely tooled mandrel and bonded together at high temperature with a thermoplastic polyurethane layer. On the inner and outer sides, the Kapton sheets have a thin aluminium coating and a thicker carbon-loaded polymer foil. This provides a certain degree of protection against discharges, and avoids the spark damages that may result from the use of a thin conductor as cathode; the added conductor improves the signal transmission along the tube. Illustrated in Figure 11.14, the straws of the forward tracker of the COMPASS spectrometer at CERN are produced with a similar technology, gluing together a 40 μm thick inner sheet of carbon-loaded polymer and a 12 μm thick aluminized polymer. At the two ends of the straw, insulating plugs, shown in Figure 11.15, provide the electrical connections and the gas distribution (Bychkov *et al.*, 2006). More than 12 000 straws, up to 320 cm in length and arranged in planar multi-layer modules, have been built and operated.

Owing to their light construction, straws are rather sensitive to humidity and temperature variations; for long tubes, regularly spaced internal supports depicted in the figure stabilize the anode wire against displacements due to mechanical or thermal deformations (Bychkov *et al.*, 2006).

The ATLAS straw-based transition radiation tracker (TRT) at CERN's LHC consists in three modules, a cylindrical barrel surrounding the central region and two forward wheels. The barrel TRT has three concentric rings, each with 32 identical straw tubes 144 cm in length and 4 mm in diameter; the two end-cap detectors are assembled in 20 wheels with short (37 cm) radially-oriented straws (Akesson *et al.*, 2004a; Martin, 2007). Embedded in foil or fibre radiators and filled with a xenon-rich gas mixture, the TRT serves the purpose of both high-resolution tracker

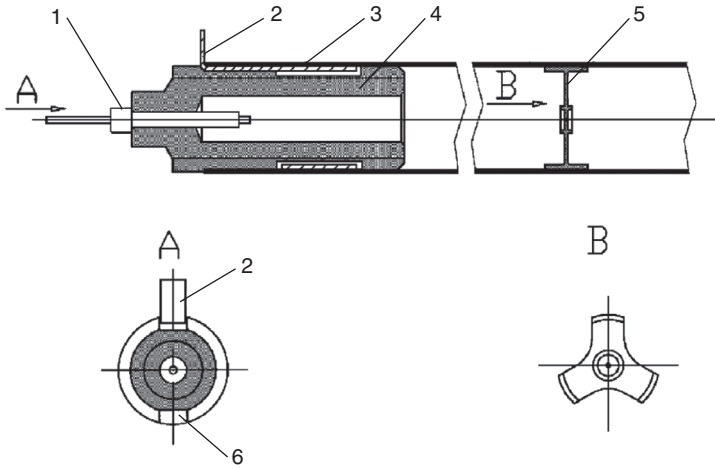


Figure 11.15 Schematics of a straw's end-plug (Bychkov *et al.*, 2006). By kind permission of Elsevier.

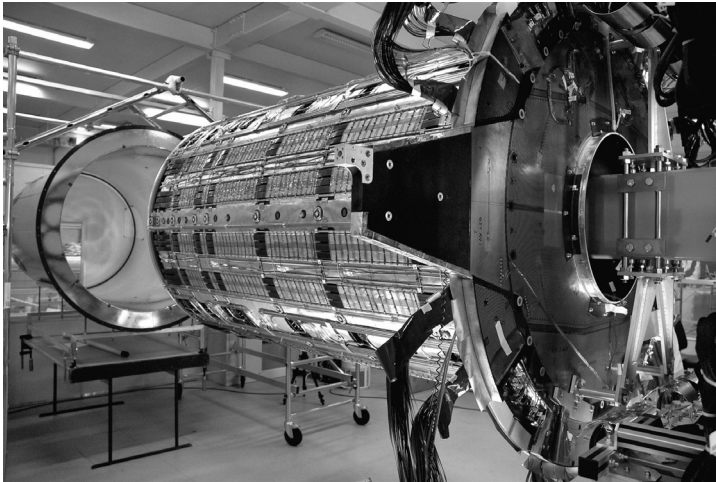


Figure 11.16 The ATLAS barrel TRT. Picture CERN (2005).

and particle identification through the detection of soft X-rays generated in the radiator by fast electrons. To improve the rate capability, anode wires are split in the middle and held together with a glass joint and are read out on both sides. Figure 11.16 and Figure 11.17 show respectively the completed barrel and end-cap TRT detectors before installation in the experiment.

Owing to the faster ion collection, due to the small diameter and higher field, straw tubes have a high intrinsic rate capability; Figure 11.18 is a measurement of relative gain on soft X-rays for a 4 mm diameter counter, and drift time resolution

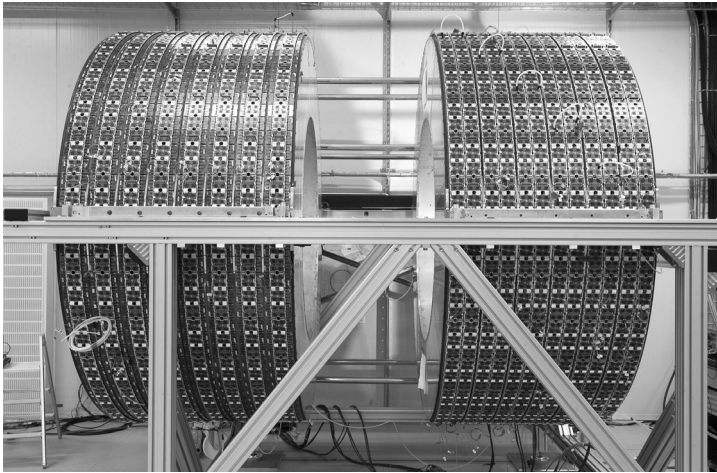


Figure 11.17 The two assembled end-cap ATLAS TRT detectors. Picture CERN (2005).

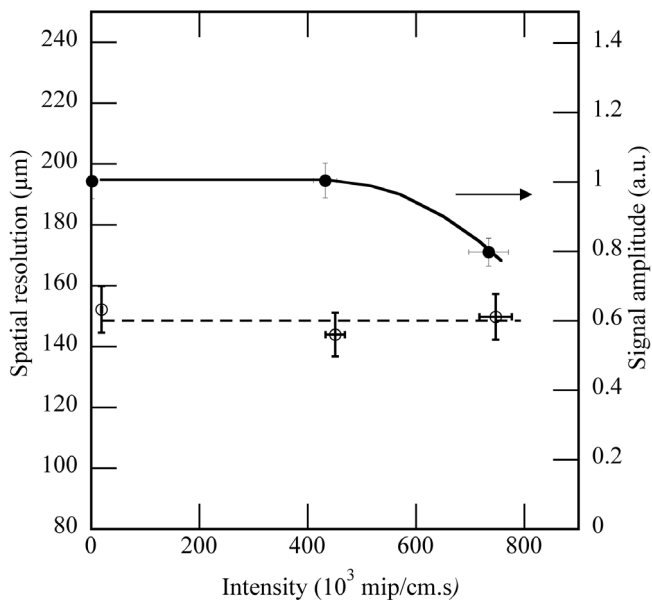


Figure 11.18 Relative gain and position accuracy as a function of particle flux (Akesson *et al.*, 1995). By kind permission of Elsevier.

for charged particles as a function of flux; the performances are unaffected up to a rate around $5 \cdot 10^5$ Hz/cm of wire (Akesson *et al.*, 1995).

As most proportional counters, straw tubes can be operated in a wide choice of filling gases; hydrocarbon mixtures are generally avoided for safety reasons and

to avoid the formation of polymers. While the straws' rate capability is limited to a few tens of kHz/mm of wire by the basic space charge processes discussed in Section 7.7, the higher granularity favours their use in high rate experiments if particular care is taken to avoid ageing problems.

Due to the manufacturing process, straws are particularly prone to suffer from the adverse effects of pollutants released by oily residues; addition of small amounts of carbon tetrafluoride can considerably extend the lifetime of the detector, thanks to its etching properties. In laboratory tests, integrated charges up to several C/cm have been reached in argon-CO₂-CF₄ without deterioration of performances (Bachmann *et al.*, 2004). However, attempts to exploit the cleaning effect of carbon tetrafluoride in the ATLAS TRT have been frustrated by the chemical aggressiveness on materials of the fluorinated compound released in the avalanches, particularly in the presence of moisture, and the use of CF₄ has been discontinued in favour of the milder cleaning action obtained with the addition of a few per cent of oxygen (Akesson *et al.*, 2002; Akesson *et al.*, 2004b). The subject of ageing and radiation damage is covered extensively in Chapter 16.

11.4 Mechanical construction and electrostatic stability

In an ideal cylindrical counter, the anode wire is in equilibrium under the effect of electrostatic forces due to the applied voltage. However, because of positioning errors, straw distortions and gravitational sag, the wire may not be perfectly centred and can move to a new equilibrium position, under the effect of the asymmetric electrostatic forces contrasted by its mechanical tension, with a maximum deflection towards the cathode in the centre. Aside from affecting the localization, the displacements reduce the difference between the voltage required for operation and the breakdown point, as shown by the measurements with several gas fillings in Figure 11.19 (Akesson *et al.*, 2004b).

Many authors have computed expressions for the conditions of wire stability under electrostatic forces, similarly to those developed for multi-wire chambers. The electrostatic force per unit length due to an offset of the wire from the centre by a quantity δ is given in MKS units by the expression (Carr and Kagan, 1986; Oh *et al.*, 1991; Akesson *et al.*, 1995):

$$F = \frac{2\pi\epsilon_0 V^2 \delta}{R^2 (\ln(R/r))^2}, \quad (11.1)$$

where V , R and r are the applied voltage, cathode and wire radius respectively. For equilibrium, the electrostatic force must be equal to or smaller than the

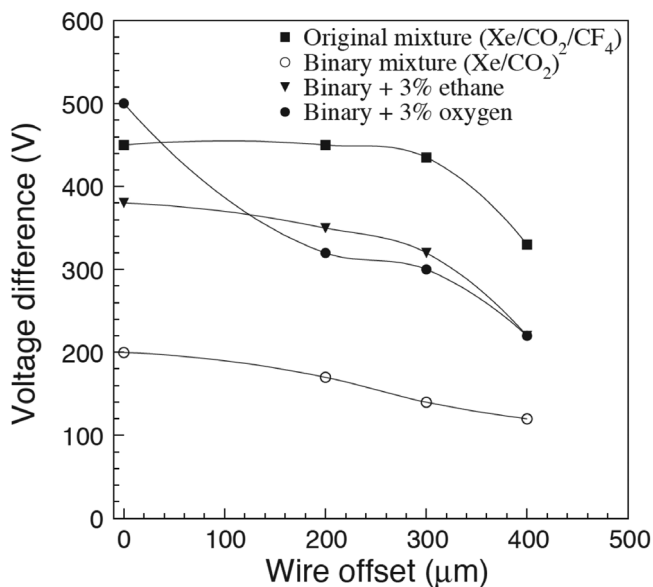


Figure 11.19 Voltage difference between operation and breakdowns as a function of wire offset in the ATLAS TRT (Akesson *et al.*, 2004b). By kind permission of Elsevier.

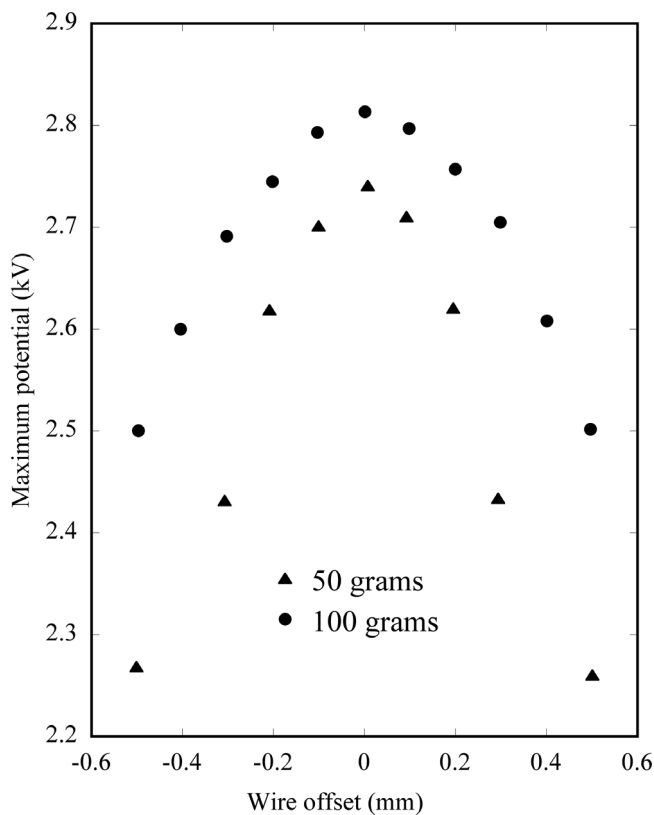


Figure 11.20 Maximum operating voltage as a function of wire offset and two values of tension (Akesson *et al.*, 1995). By kind permission of Elsevier.

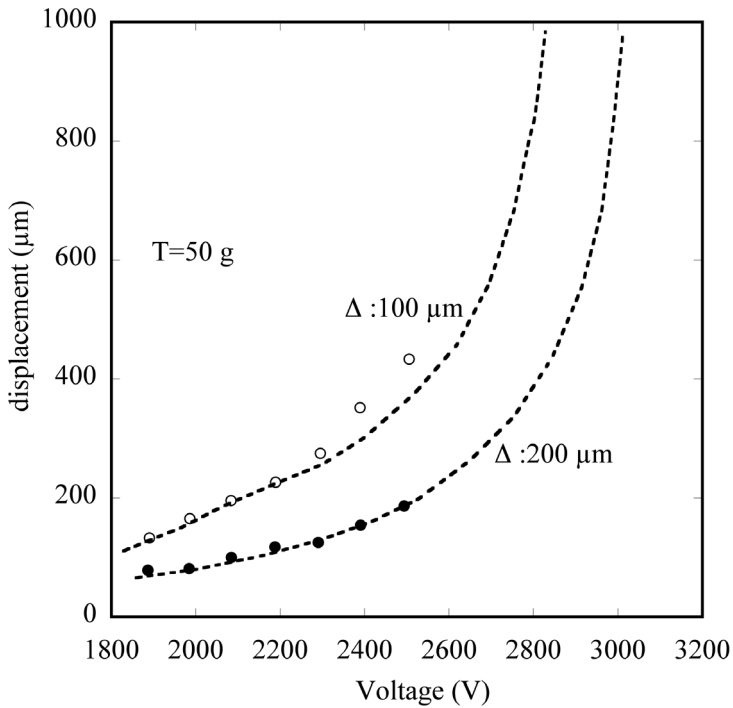


Figure 11.21 Central wire displacement as a function of voltage for two initial offsets, 100 μm (full points) and 200 μm (circles) (Ogren, 1995). By kind permission of Elsevier.

mechanical tension T of the wire; for a given tube length, this defines the maximum operating voltage:

$$T \geq \frac{2\epsilon_0 V^2 L^2}{\pi R^2 (\ln(R/r))^2}. \quad (11.2)$$

The deflection d of the midpoint of the wire of length L from its initial position is given approximately by $d = L^2 F / 8T$; breakdown will occur when the field increase due to the deflection exceeds the gas rigidity. Figure 11.20, from the last reference, shows the maximum operating voltage for a tube 1 metre long and 4 mm in diameter, filled with pure methane, as a function of the wire offset, and two values of the wire stretching tension. In Figure 11.21 the measured displacement in the centre of a wire 1 m long, stretched at 50 g is plotted as a function of voltage for two initial values of the wire offset (100 and 200 μm) (Ogren, 1995). A fit to the points is made with the expressions given in the reference.

Various types of internal wire supports or spacers have been developed to keep the maximum free length of wire below the limit of instability; one was shown in Figure 11.15.

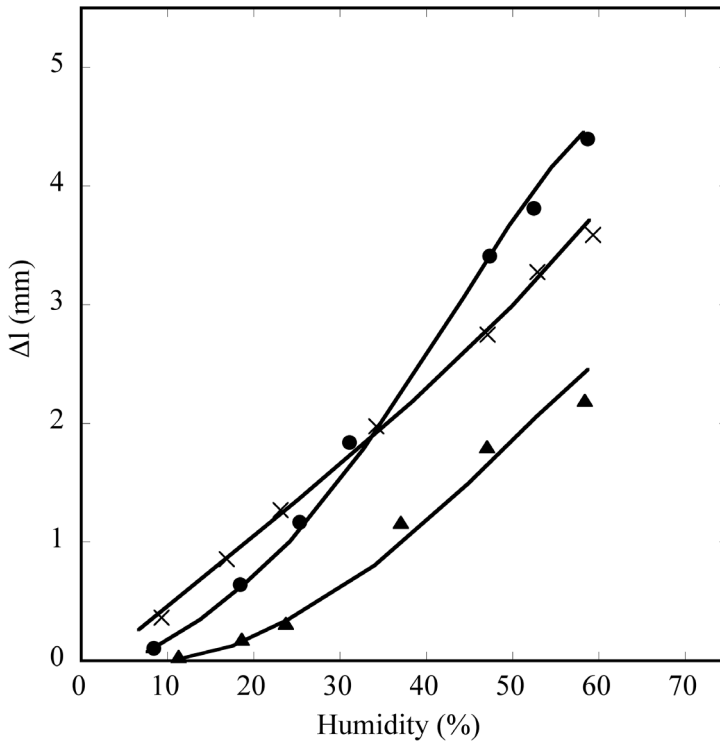


Figure 11.22 Length variations of three 3.2 m long straws as a function of humidity (Bychkov *et al.*, 2006). By kind permission of Elsevier.

The effects on the straws' mechanical properties on ambient variations, temperature and humidity have been analysed in detail; Figure 11.22 shows the elongation of 3.2 m straws made with different polymer materials as a function of relative humidity; the elongation of course affects the mechanical tension applied to the wire (Bychkov *et al.*, 2006). Similar distortions are generated by differences in the thermal expansion coefficients of the straws' components and supporting frames; this shows the importance of controlling the ambient conditions.